doi:10.1093/plphys/kiab329 PLANT PHYSIOLOGY 2021: 187: 1728–1745

Plant Physiology®

Research Article

IRONMAN tunes responses to iron deficiency in concert with environmental pH

Chandan Kumar Gautam [1,2,3] **Huei-Hsuan Tsai** [3] **and Wolfgang Schmidt** [1,3,4,5,*,†]

1 Molecular and Biological Agricultural Sciences Program, Taiwan International Graduate Program, Academia Sinica and National Chung-Hsing University, Taipei 11529, Taiwan
2 Graduate Institute of Biotechnology, National Chung-Hsing University, Taichung 40227, Taiwan
3 Institute of Plant and Microbial Biology, Academia Sinica, Taipei 11529, Taiwan
4 Biotechnology Center, National Chung-Hsing University, Taichung 40227, Taiwan
5 Genome and Systems Biology Degree Program, College of Life Science, National Taiwan University, Taipei 10617, Taiwan

*Author for communication: wosh@gate.sinica.edu.tw
†Senior author

C.K.G., H.H.T., and W.S. designed the research; C.K.G. and H.H.T. performed and analyzed experiments; W.S. and C.K.G. wrote the manuscript.
The author responsible for distribution of materials integral to the findings presented in this article in accordance with the policy described in the Instructions for Authors (https://academic.oup.com/plphys/pages/general-instructions) is: Wolfgang Schmidt (wosh@gate.sinica.edu.tw).

Abstract

Iron (Fe) is an essential mineral element that governs the composition of natural plant communities and limits crop yield in agricultural ecosystems due to its extremely low availability in most soils, particularly at alkaline pH. To extract sufficient Fe from the soil under such conditions, some plants, including Arabidopsis (*Arabidopsis thaliana*), secrete Fe-mobilizing phenylpropanoids, which mobilize sparingly soluble Fe hydroxides by reduction and chelation. We show here that ectopic expression of the peptides IRONMAN (*IMA1*) and *IMA2* improves growth on calcareous soil by inducing biosynthesis and secretion of the catecholic coumarin 7,8-dihydroxy-6-methoxycoumarin (fraxetin) via increased expression of *MYB72* and *SCOPOLETIN 8-HYDROXYLASE*, a response that is strictly dependent on elevated environmental pH (pH_e). By contrast, transcription of the cytochrome P450 family protein CYP82C4, catalyzing the subsequent hydroxylation of fraxetin to sideretin, which forms less stable complexes with iron, was strongly repressed under such conditions. We concluded that IMA peptides regulate processes supporting Fe uptake at both acidic and elevated pH by controlling gene expression upstream of or in concert with a putative pH_e signal, adapting the plant to prevailing edaphic conditions. This regulatory pattern confers tolerance to calcareous soils by extending the pH range in which Fe can be efficiently absorbed from the soil. Our results further suggest that pH_e calibrates the activities of components of the Fe deficiency response, accentuating processes that are most efficient under the prevailing conditions. Altering the expression of IMA peptides provides a route for generating plants adapted to calcareous soils.

Introduction

In natural ecosystems, growth on calcareous, that is, carbonate-rich, alkaline soils, is restricted to so-called calcicole (chalk-loving) plants, while calcifuge (chalk-fleeing) species are excluded from such habitats (Grime and Hodgson, 1969; Lee, 1998). Among other factors, the ability to thrive on calcareous substrates has been attributed to a particularly efficient strategy to extract iron (Fe), an essential mineral nutrient with extremely limited solubility in most

Received May 03, 2021. Accepted May 13, 2021. Advance access publication July 27, 2021

conditions, from the soil. In aerated soils, alkalinity decreases the availability of Fe to levels that are several orders of magnitude below the requirement of the plants (Schwab and Lindsay, 1983; Tyler, 1996). Species that are not well adapted to calcareous soils, for example, crops such as fruit trees and soybean or taxa which originate from acidic habitats, develop lime-induced chlorosis caused by insufficient uptake, maldistribution, or immobilization of Fe (Zohlen and Tyler, 2004).

The underlying causes for the superior Fe acquisition efficiency of calcicole species still remain largely enigmatic. Generally, gramineous species (Poaceae) have been regarded as being more Fe-efficient under alkaline condition than nongrasses, a distinction that has been associated with the mechanism by which Fe is mobilized by grass roots. In contrast to all other land plants, grasses have adopted a chelation-based Fe uptake system that relies on the synthesis and secretion of Fe-chelating phytosiderophores, a mechanism that has been designated as strategy II (Römheld and Marschner, 1986). Phytosiderophores are mugineic acid derivates that form soluble complexes with ferric Fe, which are fairly stable over a wide pH range (Shi et al., 1988). Conversely, nongrasses have adopted a Fe acquisition strategy which depends on the orchestrated action of enzymatic reduction of ferric chelates, H^+-ATPase-mediated acidification of the rhizosphere, and secretion of low-molecular-weight Fe-mobilizing compounds such as flavins or phenylpropanoids, a system that is referred to as strategy I (Römheld and Marschner, 1986). In Arabidopsis, chelated ferric Fe is reduced by the plasma membrane-bound FERRIC REDUCTION OXIDASE2 (FRO2; Robinson et al., 1999) and the liberated Fe^{2+} is subsequently taken up from the soil solution by IRON-REGULATED TRANSPORTER1 (IRT1; Eide et al., 1996; Vert et al., 2002). The FRO2-mediated reduction of ferric Fe is supported by proton extrusion via the P-type H^+-ATPase AHA2 (Santi and Schmidt, 2009), a process that creates a slightly acidic pH milieu in the apoplast, which is favorable for the uptake of Fe. FRO2-mediated ferric reduction is compromised at circumneutral or alkaline pH ranges (Susín et al., 1996; Lucena et al., 2007; Waters et al., 2018), rendering the strategy I system ineffective under such conditions.

In Arabidopsis, the genes mediating the Fe deficiency responses are under the control of a heterodimer consisting of the master transcription factor FER-LIKE IRON DEFICIENCY-INDUCED TRANSCRIPTION FACTOR (FIT; bHLH29) and one out of four clade Ib bHLH proteins (bHLH38, bHLH39, bHLH100, and bHLH101) (Colangelo and Guerinot, 2004; Yuan et al., 2008; Sivitz et al., 2012; Wang et al., 2013). The expression of FIT, in turn, and that of all Ib bHLH proteins, is controlled by UPSTREAM REGULATOR OF IRT1 (URI; bHLH121) in concert with IAA-LEUCINE-RESISTANT3 (ILR3; bHLH105) (Kim et al., 2019; Gao et al., 2020; Lei et al., 2020). FIT is negatively regulated by the clade IVa bHLH transcription factors bHLH18, bHLH19, bHLH20, and bHLH25 (Cui et al., 2018), and by the E3 ligases BTSL1 and BTSL2 (Rodríguez-Celma et al., 2019), which target FIT for degradation via the 26S proteasome. A recently discovered family of peptides designated IRONMAN/FE-UPTAKE-INDUCING PEPTIDE (IMA/FEP) control Fe uptake, presumably via regulation of clade Ib bHLH proteins (Grillet et al., 2018; Hirayama et al., 2018). IMA/FEP peptides are ubiquitous across land plants and share a highly conserved consensus motif at the C-terminus, which is necessary and sufficient for IMA function. The expression of *IMA1* and *IMA2* is directly controlled by bHLH121 (Gao et al., 2020). Ectopic expression of *IMA1* overrides the repression of Fe uptake by sufficient internal Fe levels, induces ferric reduction activity, and improves growth on media with low Fe solubility (Grillet et al., 2018). High ferric reduction activity is, however, insufficient to confer calcicole behavior (Schmidt and Fühner, 1998; Terés et al., 2019), indicating that other mechanisms are employed to enable plants to thrive under such conditions. Recent studies have shown that growth of nongrasses on calcareous soils requires the synthesis and secretion of species-specific, low-molecular-weight compounds, which increase the solubility of ferric hydroxides by reduction and chelation and greatly extend the pH range in which Fe can be efficiently mobilized (reviewed by Chen et al., 2017; Tsai and Schmidt, 2017; Robe et al., 2020b). In Arabidopsis, Fe deficiency triggers a massive increase in the abundance of enzymes of the phenylpropanoid pathway and an accumulation of the hydroxycoumarin scopoletin (Lan et al., 2011). Scopoletin, however, does not possess Fe-mobilizing properties, which suggests that other compounds derived from this pathway are critical for the acquisition of Fe.

The Fe(II)- and 2-oxoglutarate-dependent dioxygenase FERULOYL-COA 6′-HYDROXYLASE1 (F6′H1) catalyzes the *ortho*-hydroxylation of feruloyl-CoA into 6-hydroxyferuloyl-CoA, the first committed step in the biosynthesis of catecholic coumarins derived from scopoletin, and was identified in a genetic screen as being essential for survival on alkaline soil (Schmid et al., 2014). In the light, 6-hydroxyferuloyl-CoA is converted into scopoletin, a reaction that occurs partially spontaneously. In light-protected organs such as roots, scopoletin biosynthesis is dependent on enzymatic catalysis via COUMARIN SYNTHASE (COSY; Vanholme et al., 2019). Similar to F6′H1, COSY activity is indispensable for growth on alkaline substrates (Vanholme et al., 2019), suggesting that compounds which are produced downstream of scopoletin are required for the mobilization of Fe. Hydroxylation of scopoletin mediated by another Fe(II)- and 2-oxoglutarate-dependent dioxygenase, SCOPOLETIN 8-HYDROXYLASE (S8H), yields 7,8-dihydroxy-6-methoxycoumarin (fraxetin), a potent Fe chelator (Siwinska et al., 2018; Tsai et al., 2018, Rajniak et al., 2018). A further hydroxylation step, mediated by CYTOCHROME P450 FAMILY 82 SUBFAMILY C POLYPEPTIDE4 (CYP82C4), converts fraxetin into a novel catecholic coumarin referred to as 5,7,8-trihydroxy-6-methoxycoumarin (sideretin; Rajniak et al., 2018). Secretion of scopoletin, fraxetin, and sideretin occurs via PLEIOTROPIC DRUG

RESISTANCE9 (PDR9; Fourcroy et al., 2014; Ziegler et al., 2017; Rajniak et al., 2018).

Fraxetin and sideretin constitute the major Fe-mobilizing coumarins derived from this pathway and feature adjacent hydroxyl groups which bind Fe efficiently (Schmid et al., 2014; Rajniak et al., 2018; Tsai et al., 2018; Robe et al., 2020b). In particular, fraxetin secretion appears to be important for plant edaphic adaptation. Growth and chlorophyll content corresponded with fraxetin secretion across a suite of Arabidopsis accessions grown on high pH media with restricted Fe availability, indicating that this process is critical for the ability to thrive on alkaline soils (Tsai et al., 2018). Correspondingly, the better Fe uptake of Arabidopsis demes with high carbonate content in their native habitat relative to demes native to silicious soils was found to be due to higher proton extrusion and higher fraxetin secretion (Terés et al., 2019). Supplementing the growth media with fraxetin or growing sensitive plants from silicious soils alongside carbonate-adapted plants enhanced Fe and chlorophyll levels of the sensitive plants, underscoring a key role for Fe-mobilizing coumarins in the mobilization of Fe from recalcitrant pools (Terés et al., 2019).

Here, we set out to explore the basis on which IMA is conferring calcicole behavior to *Arabidopsis thaliana*, a calcifuge species. We demonstrate that overexpression of either *IMA1* or *IMA2* is sufficient to activate all Fe deficiency responses except for fraxetin secretion, which is modulated by the environmental hydrogen activity (pH_e). Elevated pH_e promotes the expression of *S8H* and represses the transcription of *CYP82C4*, thereby activating a separate, calcicole branch of the strategy I-type Fe deficiency response.

Results

IMA1 and IMA2 are closely co-expressed putative paralogs

IMA1 and IMA2 are highly similar peptides harboring a conserved C terminus that has been associated with Fe uptake across land plants (Grillet et al., 2018). The two peptides share 82% sequence identity and are robustly induced by Fe deficiency in both roots and shoots (Figure 1A; Rodríguez-Celma et al., 2013a, 2013b). Publicly available RNA-seq data reveal similar organ- and tissue-level expression of both genes (Supplemental Figure S1). To infer organ-specific co-expression networks around *IMA1* and *IMA2*, we downloaded and normalized a total of 5,556 RNA-seq data sets from the Sequence Read Archive hosted by the National Center for Biotechnology Information. Networks were constructed with the MACCU toolbox (Lin et al., 2011) based on pair-wise comparison of the co-expression relationships of Arabidopsis genes expressed in either roots or leaves with a Pearson coefficient >0.7 using tissue-specific data sets (1,194 for roots and 641 for leaves). In both roots and leaves, *IMA1* and *IMA2* are co-expressed with a suite of other putative or validated regulators of cellular Fe homeostasis, such as *IMA4*, *bHLH38*, *bHLH39*, *IRON-RESPONSIVE PROTEIN3* (*IRP3*; At2g14247), and *IRP6* (At5g05250; Figure 1B). Together with IMAs, IRPs were identified in transcriptional surveys as being highly Fe responsive in both roots and shoots (Figure 1A; Rodríguez-Celma et al., 2013a). IRP1 and IRP2 have been renamed to IMA1 and IMA2 after elucidation of their function (Grillet et al., 2018); the biological roles of IRP3–IRP6 remain to be elucidated. In roots, *IMA1/IMA2* is further co-expressed with *NICOTIANAMINE SYNTHASE4* (*NAS4*). In leaves, the expression of *IMA1/IMA2* is associated with *IMA3* and *bHLH100* (Figure 1B).

For further studies on the function of IMA1 and IMA2, we generated transgenic lines that expressed either gene under the control of the CaMV 35S promoter, leading to an increase in *IMA1* transcript levels between ca. 260- and 300-fold in *IMA1* overexpression lines (*IMA1ox*) and 320- to 1,500-fold of *IMA2* in *IMA2ox* lines, compared to the wild-type (Figure 1C). In wild-type plants, growth on media with restricted Fe availability (nonavailable Fe [navFe] media; 10 μM $FeCl_3$, pH 7.0) increased *IMA1* and *IMA2* expression by ca. three-fold; no further increase in IMA expression was observed in *IMA1ox* lines. Mutants harboring a defect in the expression of *F6′H1* showed >20-fold increased transcript levels of both *IMA* genes relative to wild-type plants when grown under navFe conditions, possibly reflecting a severely low Fe status of the mutant plants (Figure 1C). Notably, overexpression of either of the two *IMA* genes under study appeared to antagonize the expression of the other. A plausible explanation is that the additional Fe acquired due to the increased abundance of IMA peptides represses the transcription of other *IMA* genes, while Fe-responsive genes downstream of and dependent on IMA are still induced.

Overexpression of *IMA1/IMA2* supports Fe uptake at elevated pH

Growing plants on soil supplemented with calcium oxide (CaO) resulted in pronounced growth reduction in wild-type plants, which was more severe at higher (1%) CaO levels (Figure 2A). Plants grown on alkaline soil produced chlorotic leaves, indicative of restricted Fe availability. Mutants defective in the expression of *F6′H1* showed a more severe phenotype than the wild-type, indicating that secretion of coumarins is critical for survival under such conditions. *IMA1ox* and *IMA2ox* lines showed markedly improved growth when compared to wild-type plants, a discrepancy which was more obvious in soil supplemented with 1% CaO (Figure 2A). *IMAox* plants grown under such conditions were bigger and greener than the heavily chlorotic wild-type plants, an observation which is likely attributable to improved Fe acquisition.

Growing plants on navFe media reduced growth of the wild-type by about 40% (Figure 2, B and C). When grown on media supplemented with 50 μM Fe-EDTA at pH 5.5, *f6′h1* mutant plants were significantly bigger than the wild-type, matching previous findings (Rodríguez-Celma et al., 2013b). Growth of *f6′h1* mutants on navFe media was, however, massively impaired, leading to ∼90% decrease in shoot fresh weight (FW) at the end of the experimental period

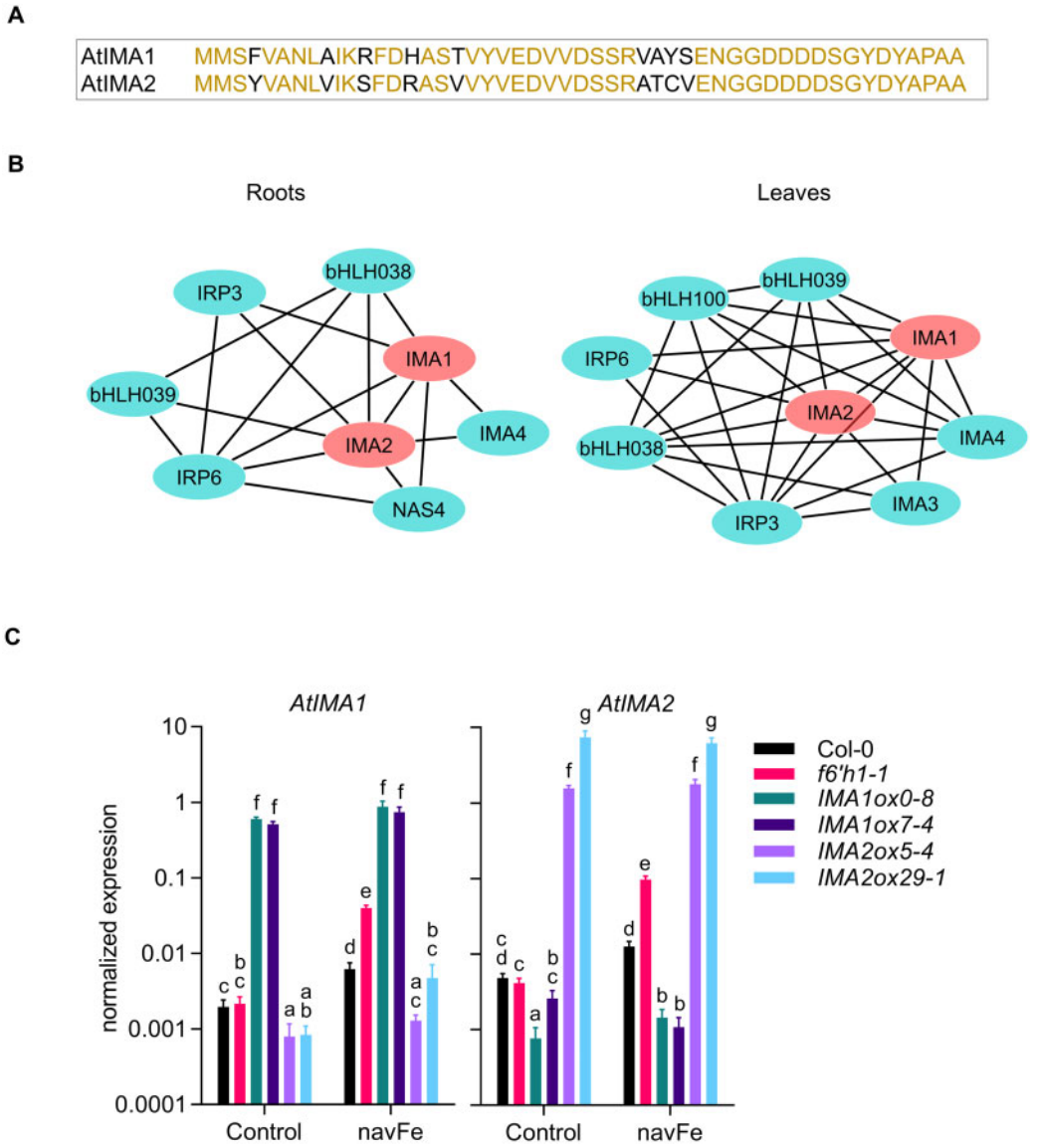

Figure 1 Sequences, co-expression networks, and expression levels of *IMA1* and *IMA2* in transgenic plants. A, Alignment of IMA1 and IMA2 peptides. Red fonts indicate identical amino acids, black fonts denote differences between the sequences. B, Co-expression networks around *IMA1* and *IMA2* in roots and leaves. Networks were constructed with the MACCU toolbox (Lin et al., 2011) against customized organ-specific databases. Genes with a Pearson coefficient of >0.7 for pairwise expression were included in the network. C, Expression of *IMA1* and *IMA2* in the wild-type, *f6′h1* mutant plants, and transgenic lines overexpressing either *IMA1* (*IMA1ox*) or *IMA2* (*IMA2ox*). Expression was measured in roots of 12-d-old seedlings grown on ES (Control) or navFe media for 3 d after 9 d of precultivation on ES media. (Each bar represents the mean ± SE of four independent experiments. Distinct letters above the bar graph indicate significant differences ($P < 0.05$) in two-way analysis of variance (ANOVA) followed by Tukey's HSD test.

(Figure 2, B and C). *IMA1/IMA2ox* lines grew slower than the wild–type under Fe-sufficient conditions (∼40% reduction in shoot FW on average), but did not show any significant growth reduction on navFe media. Octuple *ima8x* mutants, defective in the expression of all eight *IMA* genes, were highly chlorotic under all conditions, a phenotype that was more severe when grown on navFe media, where *ima8x* resembled *f6′h1* mutant plants (Figure 2, B and C). Growth on navFe media further caused a pronounced decrease in chlorophyll concentration in wild-type and, more dramatically, in *f6′h1* mutant plants. *IMA1/IMA2ox* lines exhibited a much less severe reduction in chlorophyll levels. On average, chlorophyll concentration of *IMAox* lines was decreased by 17% versus 58% in wild-type and 83% in *f6′h1* mutant plants (Figure 2D). The lowest chlorophyll concentration was observed in *ima8x* mutants (Figure 2D).

Histochemical detection of Fe by Perls staining revealed massive accumulation of Fe in roots and shoots of both *IMA1ox* and *IMA2ox* lines under Fe-sufficient conditions and when grown on media supplemented with excess Fe (400 μM Fe-EDTA), suggesting that both genes play at least partly redundant roles in the regulation of Fe uptake

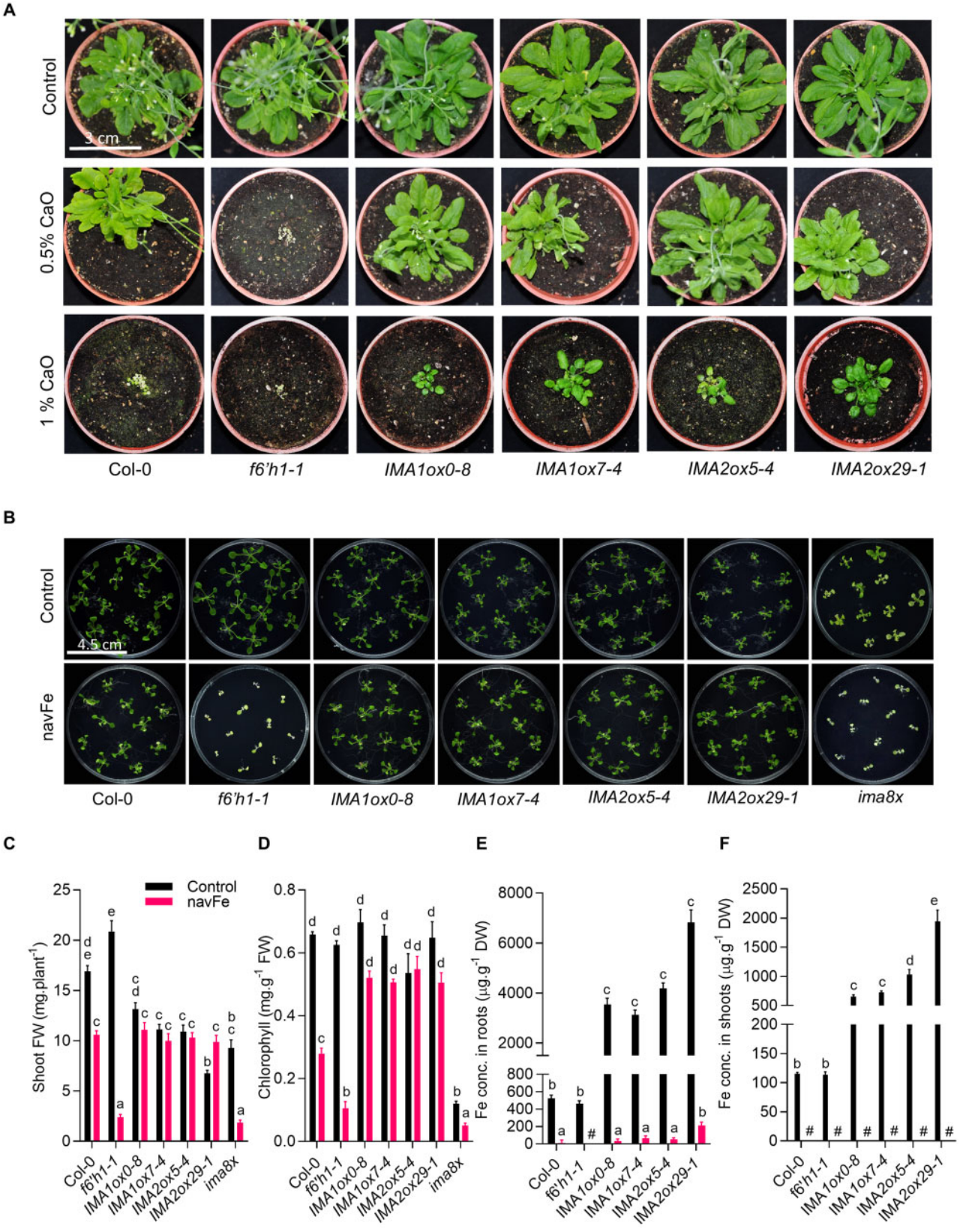

Figure 2 Overexpression of *IMA1* and *IMA2* confers tolerance to alkaline conditions. A, Phenotypes of plants grown for 8 weeks on alkaline soil supplemented with CaO. B, Phenotypes of plants grown on ES (50 µM Fe-EDTA, pH 5.5; Control) or navFe (10 µM $FeCl_3$, pH 7.0) media for 2 weeks. C, Shoot FW. D, Chlorophyll concentration. E and F, Fe concentration in roots (E) and shoots (F). DW, Dry weight; C–F, Each bar represents the mean ± SE of four (seven for shoot FW) independent experiments. Distinct letters above the bar graphs indicate significant differences ($P < 0.05$) in two-way ANOVA followed by Tukey's HSD test. Hash denotes not detected.

(Supplemental Figure S2). Growing plants on navFe media abolished Fe staining completely in both wild-type and *f6′h1* mutant plants. In *IMA1/IMA2ox* lines, staining was weak but still above the detection limit (Supplemental Figure S2), indicating that under such conditions, Fe uptake is less restricted in lines overexpressing either *IMA1* or *IMA2*. Quantifying Fe levels in the genotypes under investigation supported the semi-quantitative analysis and revealed a massive increase in root and shoot Fe concentration in *IMA1/IMA2ox* lines under Fe-sufficient conditions, relative to wild-type plants (Figure 2, E and F). When grown on navFe media, Fe was barely (in roots) or not at all (in shoots) detectable (Figure 2, E and F). These very low Fe levels were likely caused by prolonged growth on navFe media, which leads to exhaustion of the internal Fe pools. To validate the supposition that the ameliorated chlorosis of *IMA1/IMA2ox* lines grown on navFe media was due to improved Fe acquisition, we analyzed plants that were pregrown on Fe-sufficient media for 7 d and subsequently transferred to navFe media for an additional 5 d. Fe levels remained low in all genotypes under these conditions, but *IMA1/IMA2ox* lines exhibited an on average >30-fold increase in Fe levels in roots and in shoots, suggesting that IMA peptides particularly support Fe uptake under conditions of restricted Fe availability (Supplemental Figure S3).

IMA regulates Fe acquisition at different levels

To investigate the effect of IMA1 and IMA2 on the different Fe acquisition processes, we first analyzed the capacity of the lines under study to acidify the rhizosphere. Under Fe-sufficient conditions, a low constitutive acidification confined to the root tip was recorded for wild-type and *f6′h1* mutant plants; roots of *f6′h1* plants were slightly more active (Figure 3A). *IMA1/IMA2ox* lines showed a more pronounced response, covering a larger root area (Figure 3A). The enzymatic reduction of ferric chelates is a key step in the strategy I-type of Fe acquisition. In wild-type plants, in vivo Fe chelate reduction (FCR) activity was increased by seven-fold when grown on navFe media (Figure 3B). While FCR activity of *f6′h1* mutant plants was similar to wild-type plants under Fe-sufficient conditions, the mutant showed a much higher (ca. 15-fold) increase in activity when subjected to navFe conditions, possibly caused by the lack of Fe acquired via the secretion of Fe-mobilizing coumarins (Figure 3B). In both *IMA1ox* and *IMA2ox* lines, FCR activity was significantly increased under Fe-sufficient (ca. five-fold) and navFe conditions (ca. two-fold) relative to wild-type plants. Western blot analysis revealed that the Fe^{2+} transporter IRT1 is expressed at low levels under Fe-sufficient conditions, with a slight increase in *IMA1ox* and, to a lesser extent, in *IMA2ox* lines, when compared to wild-type plants (Figure 3C; Supplemental Figure S4). Under navFe conditions, the expression pattern of IRT1 protein resembled that of the in vivo FCR activity; the highest IRT1 accumulation was observed in *f6′h1* plants and *IMAox* lines (Figure 3C).

Notably, transcript levels of the master regulator *FIT* and the P-type H^+-ATPase *AHA2* did not significantly differ among the treatments or genotypes under investigation, indicative of a chiefly posttranslational regulation of gene activity (Jahn et al., 2002; Meiser et al., 2011; Figure 3D). Instead, expression of *FRO2* and *IRT1* massively increased in *IMA1/IMA2ox* lines under all Fe regimes, with higher transcript levels under navFe conditions. When grown on navFe media, *FRO2* and *IRT1* mRNA levels in *f6′h1* plants were higher than in the wild-type and were at the level of *IMAox* lines (Figure 3D). Genes encoding clade Ib bHLH proteins showed a pattern similar to *FRO2* and *IRT1*, with a significant increase in *IMAox* lines under Fe-sufficient conditions. When grown on navFe media, all genes of the Ib bHLH clade, except *bHLH101*, were expressed at significantly higher levels in *IMAox* lines when compared with the wild-type.

Together, these data show that higher IMA levels activate proton extrusion, ferric reduction, and Fe uptake at various regulatory levels and in conjunction with the Fe status of the plants. The data further indicate that the higher FRO2 activity and IRT1 protein levels of *f6′h1* mutants are insufficient for survival at elevated pH, suggesting that the secretion of Fe-mobilizing coumarins is indispensable for plants to thrive under such conditions. It can further be concluded that the improved growth of *IMAox* lines on media with low Fe availability is not solely caused by induction of the AHA2-FRO2-IRT1 module.

The composition of secreted coumarins is dependent on the pH/Fe regime

The quantities of coumarins in roots and in the media can be noninvasively approximated by detecting autofluorescence as an inherent property of some compounds such as scopoletin, scopolin, and esculin. Under Fe-sufficient conditions, only a faint signal was observed in roots of all genotypes; *IMAox* lines emitted a slightly more intense signal (Supplemental Figure S5A). When grown on navFe media, a significant increase in autofluorescence was noted for *IMA1/IMA2ox* lines relative to wild-type plants (Figure 4, A and B). In both roots and media of *f6′h1* and *ima8x* mutants, fluorescent coumarins remained below the detection limit under all conditions. Media of *IMA1/IMA2ox* lines showed not only pronounced fluorescence, but also a yellowish color, possibly attributable to the formation of fraxetin–Fe complexes (Rajniak et al., 2018; Supplemental Figure S5B).

Under Fe-sufficient conditions, targeted coumarin analysis identified scopoletin and its glycoside scopolin as the main phenolic compounds in roots. In contrast to the lack of fluorescence under Fe-sufficient conditions, *IMAox* lines showed a marked increase in the level of scopolin and scopoletin, compounds that constitute the major contributors to root fluorescence (Döll et al., 2018; Figure 4C). The lack of fluorescence in the roots under Fe-sufficient, slightly acidic conditions can be attributed to a pH-dependent shift in the spectra of fluorescent coumarins such as scopoletin, an assumption that was confirmed by UV–Vis spectroscopy (Supplemental Figure S6, A and B). When grown on navFe media, small amounts of fraxinol/isofraxidin were detected

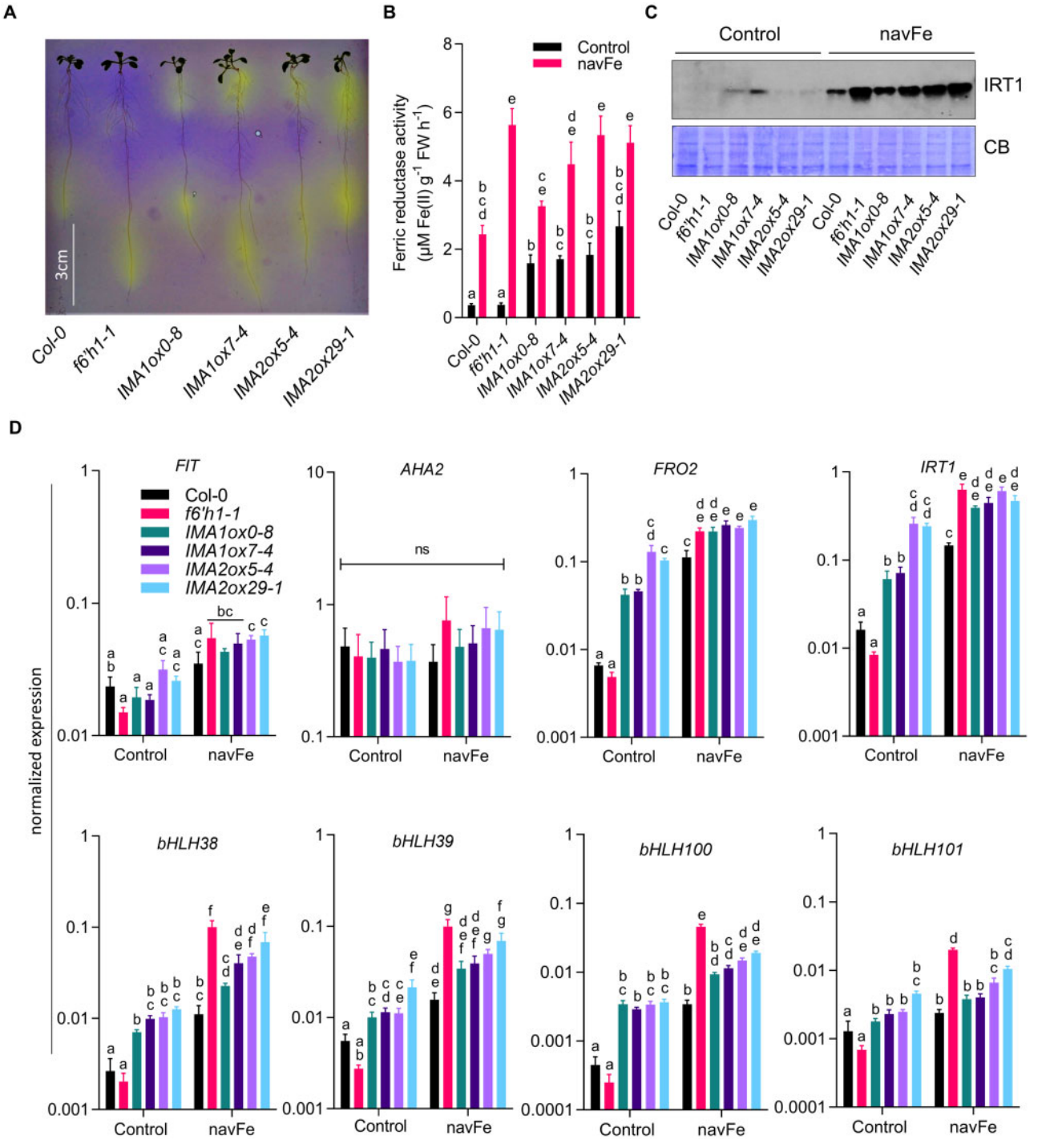

Figure 3 Fe acquisition processes are enhanced in *IMA1* and *IMA2* overexpression lines. A, Rhizosphere acidification by 8-day-old plants grown on ES media after transferring to plates containing the pH indicator bromocresol purple for 24 h. A representative image of three independent experiments is shown. Acidifcation is indicated by yellow color around the roots. B, Ferric reductase activity of 12-day-old plants grown on either ES (Control) or navFe media for 3 days, after 9 days of precultivation on ES media. C, Level of IRT1 protein (~34 kDa) in root samples from 12-day-old plants grown on either ES or navFe media for 3 days, after 9 days of precultivation on ES media. Coomassie blue (CB) was used as loading control. Per lane, 10 μg of total protein was loaded. An image representative of three independent experiments is shown. D, Expression of major Fe uptake genes in roots of 12-day-old seedling grown on ES or navFe media for 3 days, after 9 days of precultivation on ES media. Gene expression was determined by RT-qPCR using ΔC_T method and expression of elongation factor 1 alpha as an internal control. Each bar in (B) and (D) represents the mean ± SE of four independent experiments. Distinct letters above the bar graph indicate significant differences ($P < 0.05$) in two-way ANOVA followed by Tukey's HSD test.

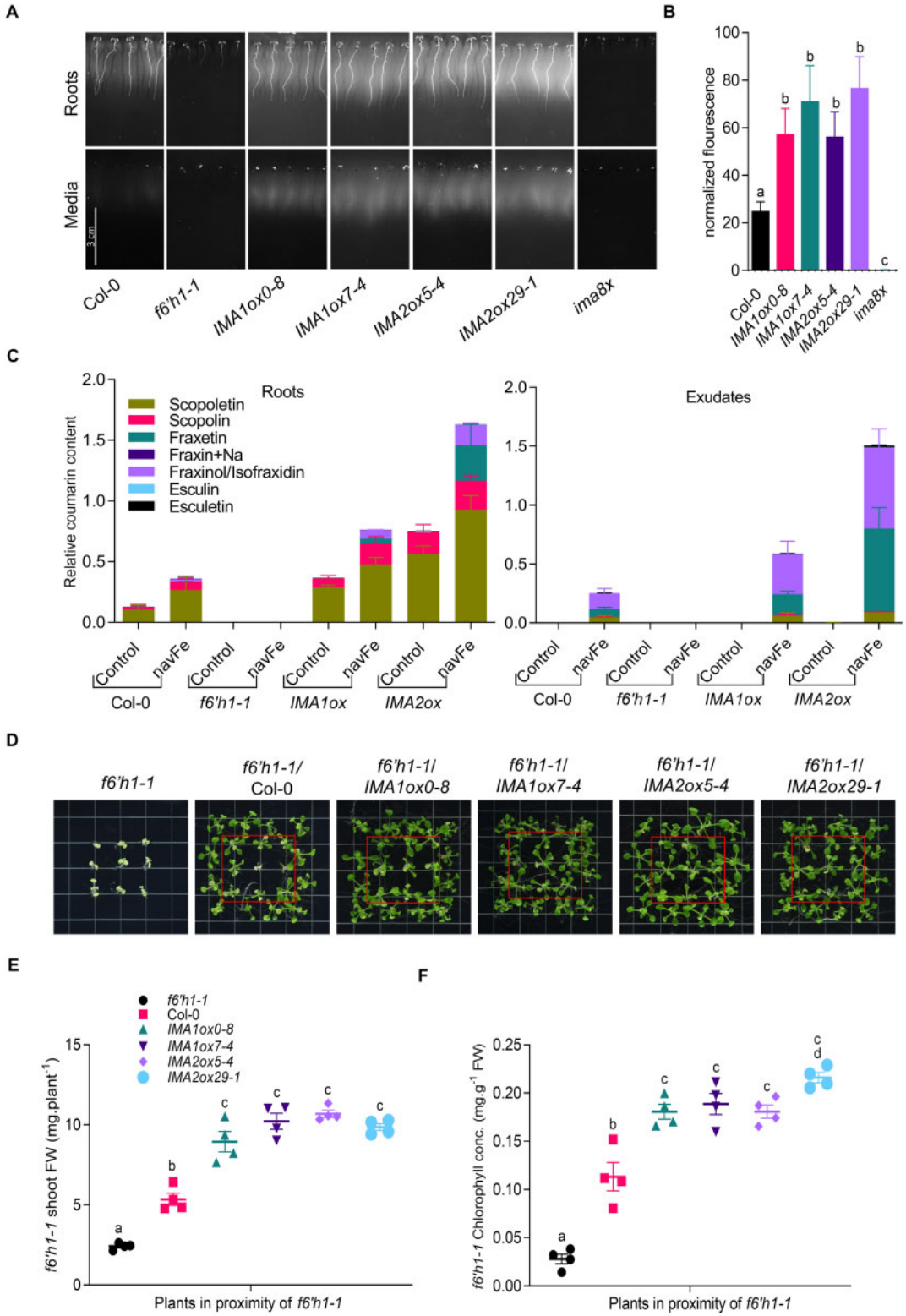

Figure 4 Overexpression of *IMA1* and *IMA2* supports the secretion of Fe-mobilizing coumarins under navFe conditions. A, Accumulation of fluorescent coumarins in roots and media of 7-d-old plants grown on navFe media. Photos were captured using 365 nm as the excitation wavelength, before and after removing plants from the media. Representative images of three independent experiments are shown. B, Quantification of root exudate fluorescence. Each bar represents the mean ± SE of four independent experiments. Distinct letters above the bar graph indicate significant differences ($P < 0.05$) in one-way ANOVA followed by Tukey's HSD test. C, Relative abundance of selected coumarins in roots and exudates of plants grown on ES (Control) or navFe media. Bars represent the relative content of different coumarin compounds presented as peak area normalized to the number of roots and internal standard peak area. Values are mean relative coumarin content ± SE obtained from three independent experiments. For coumarin extraction from roots, circa 20 plants were used for each replicate. D, Rescue of the phenotype of *f6′h1-1* mutant plants (in red boxes) by wild-type, *IMA1ox*, or *IMA2ox* plants grown alongside mutant plants on navFe media. Representative images of four independent experiments are shown. E, Shoot FW of rescued *f6′h1-1* plants. F, Total chlorophyll concentration of leaves from rescued *f6′h1-1* plants. Grouped interleaved scatter plot show SEM of the replicates.

in the wild-type in addition to scopolin and scopoletin, which account for the largest part of the detected coumarins. In roots of *IMA1/IMA2ox* lines, all identified coumarins were increased relative to the wild-type, including the Fe-mobilizing compound fraxetin, which was detectable only in very low quantities in the wild-type. *IMA1ox* and *IMA2ox* lines accumulated 28- and 200-fold more fraxetin in the roots than the wild-type, respectively (Figure 4C).

As for exudates, fraxinol/isofraxidin and fraxetin were the most prominent compounds for wild-type plants, and scopoletin was detected in minor amounts. Similar to what was observed in roots, media of *IMA1/IMA2ox* lines contained much higher levels of coumarins than that of wild-type plants, and this effect was particularly pronounced when fraxetin levels are considered. *IMA1ox* and *IMA2ox* lines secreted 3- and 10-fold more fraxetin into the media than wild-type plants, an observation which matches the better performance of these lines on alkaline soil. In contrast, scopoletin levels did not differ much among the lines, except for *f6′h1* mutants, which neither produced nor secreted any detectable amount of the coumarins covered in the analysis (Figure 4C). The difference in fraxetin secretion between wild-type plants and *IMA1/IMA2ox* lines was also observed in experiments aimed at rescuing the mutant phenotype of *f6′h1* plants. Growing *f6′h1* mutant plants alongside Columbia-0 (Col-0) doubled the shoot FW and increased chlorophyll concentration of the mutant by approximately four-fold (Figure 4, D–F). Replacing wild-type plants with *IMA1/IMA2ox* lines further improved growth and chlorophyll concentration of *f6′h1* plants, supporting the notion that the coumarins secreted by *IMA1/IMA2ox* lines are biologically active and qualitatively or quantitatively superior to those of the wild-type (Figure 4, D–F).

Together, these data indicate that secretion of Fe-mobilizing compound requires an unidentified Fe deficiency/high pH signal; in contrast to the pronounced induction of proton extrusion, FCR activity, and IRT1 accumulation in the presence of Fe, no coumarins are secreted by *IMA1/IMA2ox* lines under Fe-sufficient conditions.

The expression of genes involved in coumarin biosynthesis is controlled by pH_e and Fe

To further investigate the importance of the Fe/pH regime for the secretion of coumarins, we determined the transcript levels of genes involved in coumarin secretion under Fe-sufficient (pH 5.5) and navFe conditions (pH 7.0). Under Fe-sufficient conditions, the expression of *F6′H1* did not change in lines overexpressing *IMA1/IMA2*, relative to wild-type plants (Figure 5A). Growing plants on navFe media increased *F6′H1* mRNA levels significantly, with no apparent differences among the genotypes, except for *f6′h1* mutant plants, which showed low transcript levels under all conditions. Expression of *S8H*, which mediates the conversion of scopoletin to fraxetin, was increased by overexpression of *IMA* under Fe-sufficient conditions, and strongly induced in all lines under navFe conditions, with higher expression in all *IMAox* lines relative to wild-type plants. Conspicuously, an increase in *S8H* transcript levels relative to wild-type plants was also observed in *f6′h1* mutants under navFe, but not under Fe-sufficient conditions, possibly due to more depleted Fe levels of the plants under these conditions (Figure 5A). The strong induction of *S8H* was consistent with higher accumulation of S8H protein in the *f6′h1* mutant and *IMAox* lines (Figure 5B; Supplemental Figure S4). While overexpression of *IMA1* and *IMA2* highly increased *CYP82C4* transcript levels under (acidic) Fe-sufficient conditions, such an increase was observed neither in wild-type nor in *IMAox* plants when plants were grown under navFe conditions. Instead, in all lines transcription remained at the low levels observed under control conditions (Figure 5A).

The expression pattern of *MYB72*, a transcription factor that is critical for growth under Fe-limiting, alkaline conditions (Palmer et al., 2013), resembled that of *S8H*, except for a lack of pronounced induction of *MYB72* by overexpression of *IMA1/IMA2* under Fe-sufficient conditions (Figure 5A). Induction of the MYB72-dependent *BETA GLUCOSIDASE42* (*BGLU42*), which mediates the deglycosylation of scopoletin, and possibly other coumarin glycosides, as a necessary step before secretion into the rhizosphere (Zamioudis et al., 2014), was observed under navFe conditions, but *BGLU42* transcript levels did not differ among the genotypes when grown on Estelle and Somerville (ES) media. No statistically significant changes were observed for the expression of the coumarin exporter *PDR9*, although a trend toward higher transcript levels was observed under navFe conditions (Figure 5A).

Environmental pH modulates gene transcription

To distinguish the effect of pH_e from that of Fe availability, we determined the transcript levels of genes involved in the secretion of Fe-mobilizing coumarins at various Fe/pH regimes. The activity of Fe in the media is dependent on the stability of the Fe compound, which in turn is strongly affected by pH. To account for this effect, we grew plants on Fe-deficient media (+ferrozine), and media supplemented with various Fe sources, including Fe-EDTA (unstable at elevated pH), Fe-ethylenediamine-N,N′-bis (FeEDDHA; stable over the pH range under investigation), $FeCl_3$ (low solubility particularly at elevated pH), and precipitated $Fe(OH)_3$ (very low solubility over the whole pH range; Boxma, 1981; Norvell, 1991; Lucena and Chaney, 2006). Seedlings grown on media containing Fe sources that are stable at elevated pH (FeEDDHA or Fe-EDTA) showed no or very mild chlorosis and no changes in Fe concentration when compared to plants grown at pH 5.5. However, supplementing the media with $FeCl_3$ caused dramatic decreases in chlorophyll levels and Fe concentration (Supplemental Figure S7). At pH 5.5, expression of *MYB72* was strongly induced by Fe deficiency and, to a lesser extent, by low Fe availability (Figure 6A). At pH 7.0, *MYB72* transcript levels were much higher under all conditions, except for Fe-deficient media where expression appears to reach maximum transcription rates which cannot be further enhanced. All coumarin-related genes showed the

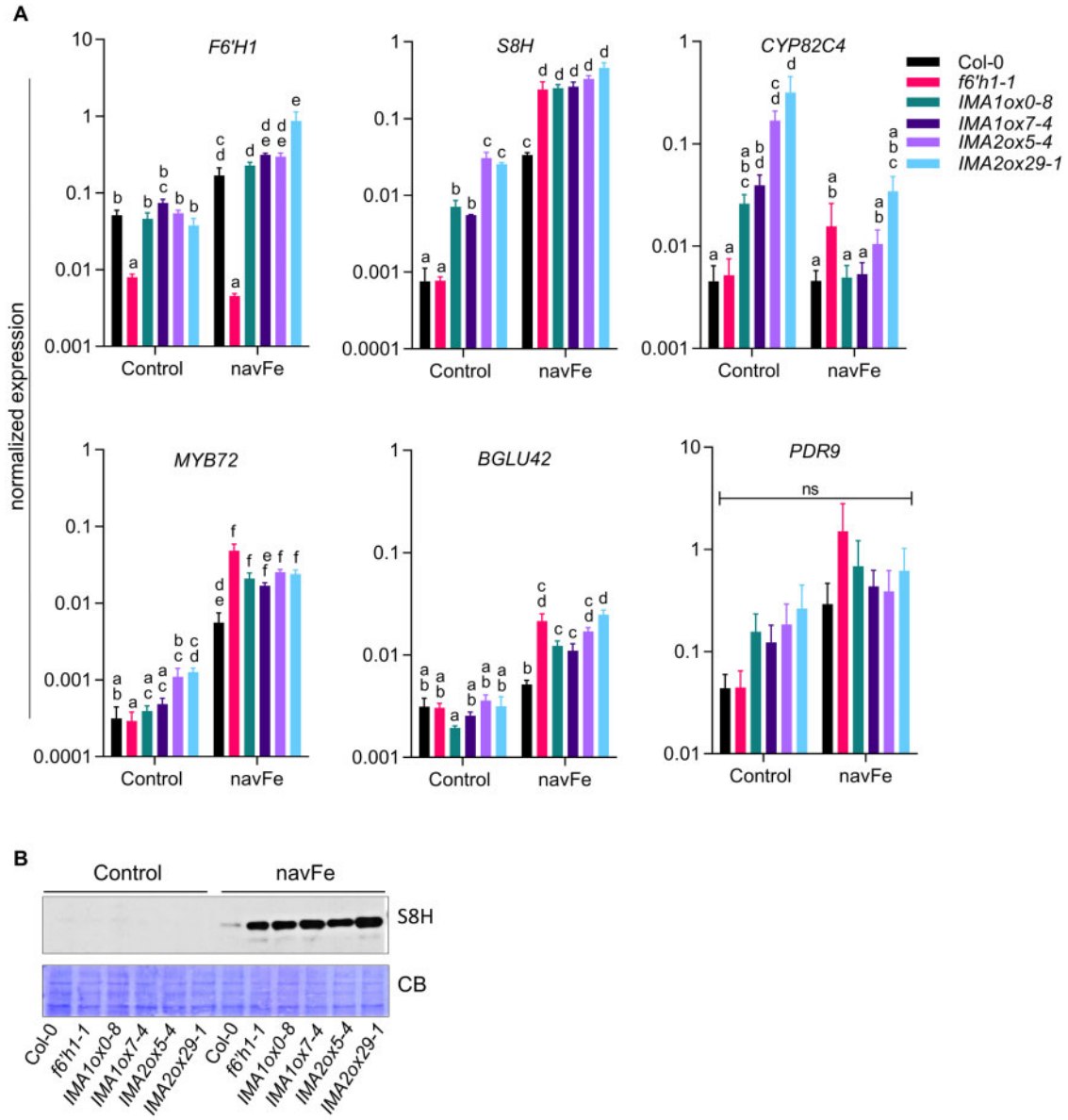

Figure 5 Expression of coumarin biosynthesis-related genes in *IMA1*/*IMA2ox* lines. RT-qPCR analysis of gene expression in roots of 12-d-old seedlings grown on ES (Control) or navFe media for 3 d, after 9 d preculture on ES media. Gene expression was determined using the ΔC_T method with elongation factor 1 alpha as an internal control. Each bar represents the mean ± SE of four independent experiments. Distinct letters above the bar graph indicate significant differences ($P < 0.05$) in two-way ANOVA followed by Tukey's HSD test. B, Level of S8H protein (~40 kDa) in root samples from 12-d-old plants grown on either ES or navFe media for 3 d, after 9 d of precultivation on ES media. CB was used as loading control. Per lane, 10 μg of total protein was loaded. An image representative of three independent experiments is shown.

highest transcript levels on Fe-deficient media. The transcription of *BGLU42*, *F6′H1*, and *COSY* was not much affected by the various growth conditions (Figure 6A). Instead, *S8H* expression was strongly induced by Fe deficiency at pH 5.5 and by supplementing the media with $FeCl_3$ or $Fe(OH)_3$ (Figure 6A). Growth on media with elevated pH increased the message levels of *S8H* under all conditions (except for Fe-deficient media), particularly when plants were grown on media supplemented with less soluble Fe compounds. Generally, the *S8H* expression pattern resembles that of *MYB72* (Figure 6A). Western blot analysis mirrored the high induction of *S8H* by Fe deficiency at both acidic and elevated pH and the pH-dependent expression in all treatments, with protein abundance increasing with decreasing stability of the added Fe compounds (Figure 6B). While expression of *CYP82C4* showed a pattern similar to that of *S8H* at pH 5.5, growth at pH 7.0 strongly downregulated transcript levels in all treatments (Figure 6A). Although inducibility by Fe deficiency was still observable at neutral pH, expression levels of *CYP82C4* were >600-fold lower at pH 7.0 when compared to pH 5.5, suggesting that at elevated pH, fraxetin is favored over sideretin production. The expression of *FIT*, *IMA1*, and *IMA2* was not much affected by the Fe/pH regimes under study, except for a strong induction of

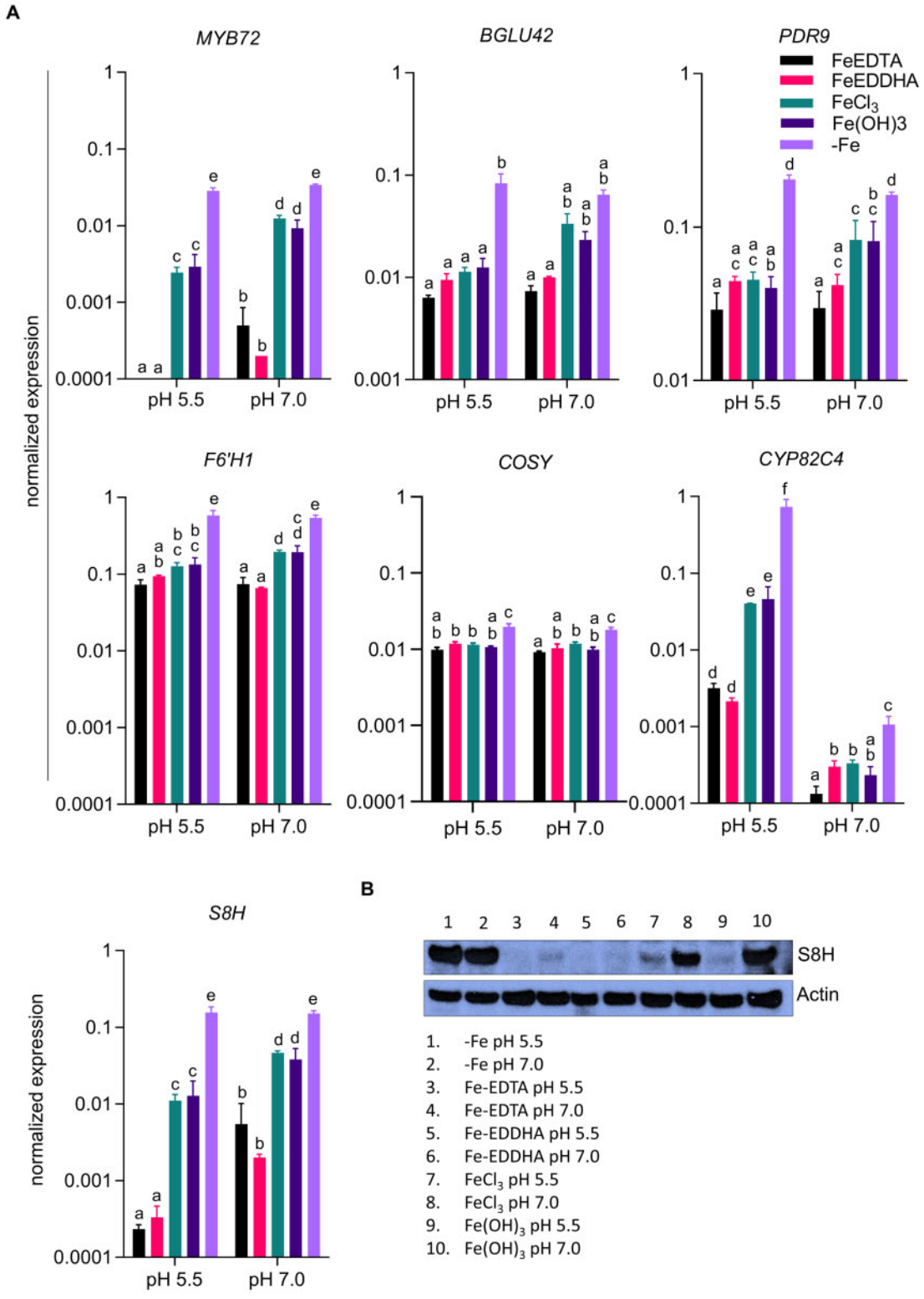

Figure 6 Media pH and Fe availability control the expression of coumarin-related genes. Plants were directly germinated for 14 d on either Fe-deficient media (with 120 μM ferrozine) or media supplemented with either Fe-EDTA (40 μM), FeEDDHA (40 μM), $FeCl_3$ (40 μM), or precipitated $Fe(OH)_3$ (40 μM) at pH 5.5 or pH 7.0. A, Expression of *MYB72*, *BGLU42*, *PDR9*, *F6′H1*, *COSY*, *CYP82C4*, and *S8H* in roots. Gene expression was determined using the ΔC_T method with elongation factor 1 alpha as an internal control. Each bar represents the mean ± SE of three independent experiments. Distinct letters above the bar graph indicate significant differences ($P < 0.05$) in two-way ANOVA followed by Tukey's HSD test. B, Expression of S8H protein (~40 kDa) in root samples. Actin (~45 kDa) was used as loading control. Per lane, 20 μg of total protein were loaded. An image representative of three independent experiments is shown.

all three genes by the absence of Fe, which was not influenced by pH. Interestingly, expression of *IMA3* showed a different pattern, being strongly repressed by stable Fe compounds (Fe-EDTA and Fe-EDDHA) at elevated pH (Supplemental Figure S8). This decrease at elevated pH, albeit less pronounced, was also observed for *IMA1* and *IMA2* when grown on media supplemented with Fe-EDDHA.

In conclusion, the results from these experiments suggest that depending on the external pH, *IMA1*/*IMA2* support the biosynthesis and secretion of different coumarins. Under acidic conditions, sideretin production is favored through upregulation of both *S8H* and *CYP82C4*. At elevated pH and in the absence of available Fe, *S8H* is highly induced while *CYP82C4* expression is strongly repressed, supporting the production of fraxetin, which forms more stable complexes with Fe under such conditions.

Discussion

IMA overexpression confers calcicole behavior

The Arabidopsis genome harbors eight *IMA* genes, of which only two (*IMA1*/*FEP3* and *IMA3*/*FEP1*) have been functionally explored (Grillet et al., 2018; Hirayama et al., 2018). IMA1 and IMA2 share an identical C-terminal consensus motif characteristic of all IMA peptides across angiosperms, exhibit similar expression patterns, and induce Fe acquisition responses in a similar manner and to a comparable extent, suggesting that the two genes are to a large degree genetically redundant. In leaves, *IMA1* and *IMA2* are tightly co-expressed with *IMA4* and genes that have been associated with cellular Fe homeostasis. Notably, in roots, expression of *IMA1/2* is closely associated with *NAS4*, a putative target of MYB72 (Palmer et al., 2013). Homozygous *myb72* and *nas4* mutants display similar phenotypes, featuring lower chlorophyll and decreased Fe levels when compared with the wild-type. Overexpression of *NAS4* rescued *myb10myb72* mutants (Palmer et al., 2013), indicating that NAS4 is of particular importance for the adaptation to alkaline conditions with low Fe availability.

The enzymatic reduction of ferric chelates is the rate-limiting step of strategy I-type Fe uptake, and determines the efficiency by which Fe is taken up (Grusak et al., 1990). Under Fe-sufficient (and slightly acidic) conditions, elevated IMA levels increase the expression of *FRO2* and in vivo FCR activity, which is causative for increased Fe levels in all plant parts, including seeds (Grillet et al., 2018). However, activated FCR activity and increased proton extrusion of *f6′h1* plants are insufficient to alleviate the pronounced growth inhibition of the mutant on media with elevated pH, indicating that the secretion of Fe-mobilizing coumarins is indispensable under such conditions. In *IMAox* lines, fraxetin secretion was massively increased under permissive conditions (low Fe status of the plants and elevated pH), an increase that was much more pronounced than that observed for other Fe acquisition responses. Conspicuously, under Fe-sufficient conditions, an IMA-dependent induction was observed for the synthesis of scopolin and scopoletin but not for fraxetin, indicating that IMA-mediated fraxetin production requires both a low Fe status and high pH_e, thereby prioritizing the secretion of fraxetin over that of the upstream (scopoletin) and downstream products (sideretin). At elevated pH, a concurrent, unweighted induction of all steps of the coumarin pathway may be counterproductive for Fe acquisition, since sideretin secretion will reduce fraxetin levels and thus compromise the mobilization of Fe from recalcitrant pools in soils.

Similar to *IMAox* lines, in wild-type plants, the most pronounced accumulation and secretion of fraxetin was observed under the combined influence of elevated pH_e and Fe deficiency; no such pattern was observed for scopoletin (Sisó-Terraza et al., 2016). A pH-dependent increase in the secretion of phenolic compounds was also reported for soybean and mung bean plants (Waters et al., 2018; Nair et al., 2020), suggesting that the pH response is conserved in some, if not most, nongrass species. We show here that in the presence of the pH-stable Fe source Fe-EDDHA, an increase in media pH from 5.5 to 7.0 led to a markedly higher (ca. six-fold on average) expression of *S8H*. Under similar conditions, *CYP82C4* transcript levels were decreased by the same factor. At elevated pH, the Fe deficiency-induced expression of *CYP82C4* was compromised, amplifying the difference in transcript levels between pH 5.5 and pH 7.0 by >600-fold. Similar to elevated pH ranges, under acidic conditions, an indiscriminate induction of all steps of the coumarin biosynthetic pathway would be disadvantageous for plant fitness; fraxetin synthesis would cause an unfavorable decrease of the phytoalexin scopoletin and decrease the production of sideretin, which would deplete the amount of chelated Fe as a substrate for FRO2-mediated ferric reduction. It should be noted that the expression of both *S8H* and *CYP82C4* is controlled by FIT (Colangelo and Guerinot, 2004) and inducible by Fe deficiency at the transcript and protein level under acidic conditions (Lan et al., 2011; Grillet et al., 2018). This finding implies that *trans*-acting factors can modulate or abolish FIT-dependent induction in response to pH_e. In contrast to yeast, where ambient pH is perceived by a sensor complex at the cell surface and communicated via a well-described signaling cascade to drive the expression of genes adapting the cell to an alkaline environment (Obara and Kihara, 2014; Peñalva et al., 2014), such pH_e signaling has not yet been described in plants (Raven, 1990; Tsai and Schmidt, 2021). However, changes in media pH were shown to rapidly and thoroughly alter gene expression profiles in Arabidopsis roots, strongly suggesting that plants are capable of monitoring and responding to changes in pH_e (Lager et al., 2010; Tsai and Schmidt, 2020). It is noteworthy that some of the genes under study did not show sensitivity toward changes in environmental pH, excluding nonspecific secondary effects of pH_e on gene expression.

Fe deficiency responses fractionate into a calcifuge and a calcicole branch

The strategy I-type Fe deficiency response constitutes a cooperative entity, which orchestrates Fe acquisition processes

at low Fe availability. Our data imply that different branches of the Fe deficiency syndrome are calibrated in a pH_e-dependent manner, accentuating processes that are most efficient under a given set of edaphic conditions (Figure 7). The balance between the two branches of the Fe deficiency response is tipped by the pH_e, inducing a "calcifuge" suite of processes at acidic pH, and a "calcicole" response at elevated pH. Under acidic conditions, Fe is mainly acquired via enzymatic reduction and taken up through FRO2/IRT1. It can be assumed that CYP82C4 activity and sideretin production are closely associated with the AHA2-FRO2-IRT1 module, a supposition that is corroborated by the extremely close correlation of *IRT1* and *CYP82C4* expression (http//:atted.jp), and the identification of CYP82C4 as a potential interactor of IRT1 (Martín-Barranco et al., 2020). Sideretin exhibits maximal Fe-mobilizing pH capacity at lower pH ranges when compared to fraxetin (Rajniak et al., 2018; Tsai et al., 2018), implying that sideretin secretion is part of the calcifuge branch. A pH-dependent prioritization of the Fe acquisition process is of ecological importance, since it profoundly increases the range of hydrogen activities in which Fe can be assimilated from the soil.

The transcription factor *MYB72* was found to be critical for growth on alkaline soil (Palmer et al. 2013). In this study, we show that *MYB72* expression is highly pH-dependent, exhibiting a pattern similar to *S8H* but contrary to *CYP82C4*, which places MYB72 in the calcicole branch of the response. The β-glucosidase *BGLU42* is a putative target of MYB72 (Palmer et al., 2013), is highly responsive to Fe deficiency (Grillet et al., 2018), and was shown to deglycosylate scopolin (Ahn et al., 2010; Stringlis et al., 2018). Interestingly, under navFe conditions, overexpression of *IMA1/2* significantly increases *BGLU42* expression relative to wild-type plants (Figure 5), while the expression of three other scopoletin-hydolyzing β-glucosidases from the same clade, *BGLU21*, *BGLU22*, and *BGLU23*, was decreased under such conditions (Ahn et al., 2010; Tsai and Schmidt, 2020). Moreover, *BGLU21* and *BGLU22* are downregulated in *IMA1ox* lines under Fe-deficient conditions (Grillet et al., 2018), suggesting that BGLU42 could be involved in the deglycosylation of coumarins, including fraxetin, at elevated pH_e. It may thus be assumed that high pH triggers a module of the Fe-deficiency response that comprises *MYB72*, *S8H*, and *BGLU42*, which supports the secretion of fraxetin and confers calcicole behavior (Figure 7). An open question is whether secreted coumarins can be transported back into the cell together, either as such or as a complex with Fe. Uptake of the secreted coumarins, analogously to phytosiderophores released by grasses, would be ecologically advantageous in view of energy conservation and the low efficiency of enzymatic Fe^{3+} reduction at neutral or alkaline pH. Glycosylated coumarins were detected in *f6′h1* plants when grown alongside wild-type plants, or when scopoletin, esculetin, or fraxetin was provided exogenously, suggesting that coumarins can be taken up and stored as glycosides in the vacuole (Robe et al., 2020a). Whether or not the coumarins taken up from the soil solution can be transported into the cell as coumarin–Fe complex by an auxiliary Fe uptake system remains to be elucidated.

Conclusions

In summary, we show here that high IMA1/IMA2 levels partly overrule the downregulation of Fe uptake at sufficient internal Fe levels and induce rhizosphere acidification, Fe^{3+} reduction, Fe^{2+} uptake, and the biosynthesis and secretion of scopoletin by acting as transcriptional activators. A complex, pH-dependent regulation was observed for the secretion of Fe-mobilizing catecholic coumarins, prioritizing the production of fraxetin over sideretin at elevated pH. Notably, at elevated pH, *f6′h1* (defective in secreting catecholic coumarins) and *ima8x* mutants (defective in all Fe deficiency responses) showed similar phenotypes, indicating that a functional AHA2-FRO2-IRT1 module is insufficient to enable growth under such conditions.

Root-secreted coumarins not only act directly on Fe uptake via mobilization of recalcitrant Fe pools, but also indirectly by retracting pathogens and attracting beneficial bacteria, which in turn improve the access to mobile Fe in soils (Stringlis et al., 2019; Voges et al., 2019; Harbort et al., 2020). While such beneficial effects on plant growth were shown for scopoletin and fraxetin, sideretin does not appear to play such a role (Harbort et al., 2020). It may be concluded that the dual function of fraxetin in Fe acquisition is critical for conferring fitness at elevated pH. Manipulating the expression of IMA/FEP peptides constitutes a promising approach to generate germplasm adapted to low Fe availability. Ectopic expression of *IMAs* results in an increase in Fe in both strategies I and II crops such as rice (*Oryza sativa*) and tomato (*Solanum lycopersicum*), with increased Fe content in grains and fruits, respectively (Grillet et al., 2018; Kobayashi et al., 2020), making IMAs a promising candidate for improving Fe acquisition of virtually all crops. In particular, crops grown on calcareous soils may profit from improved growth and nutritional quality of edible plant parts.

Materials and methods

Plant materials and growth conditions

Seeds of Arabidopsis (*A. thaliana* (L.) Heynh) accession Col-0 and *f6′h1-1* (Salk_132418C) T-DNA insertion mutants were obtained from the Arabidopsis Biological Resource Center (Ohio State University). The lines carrying *CaMV* $_{pro}$*35S::IMA1*, and *ima8x* octuple mutants have been described previously (Grillet et al., 2018). *Agrobacterium tumefaciens*-mediated transformation (Clough and Bent, 1998) was used to transform wild-type plants with pH2GW7 (obtained from the VIB-UGent Center for Plant Systems Biology) containing CaMV 35S promoter-driven *IMA2* CDS (using the primers listed in Supplemental Table S1), yielding *IMA2* overexpression lines. Overexpression in transgenic plants was confirmed by RT-qPCR. Plants were grown in a growth chamber on solid nutrient media as described by Estelle and Somerville (1987) (ES media), composed of

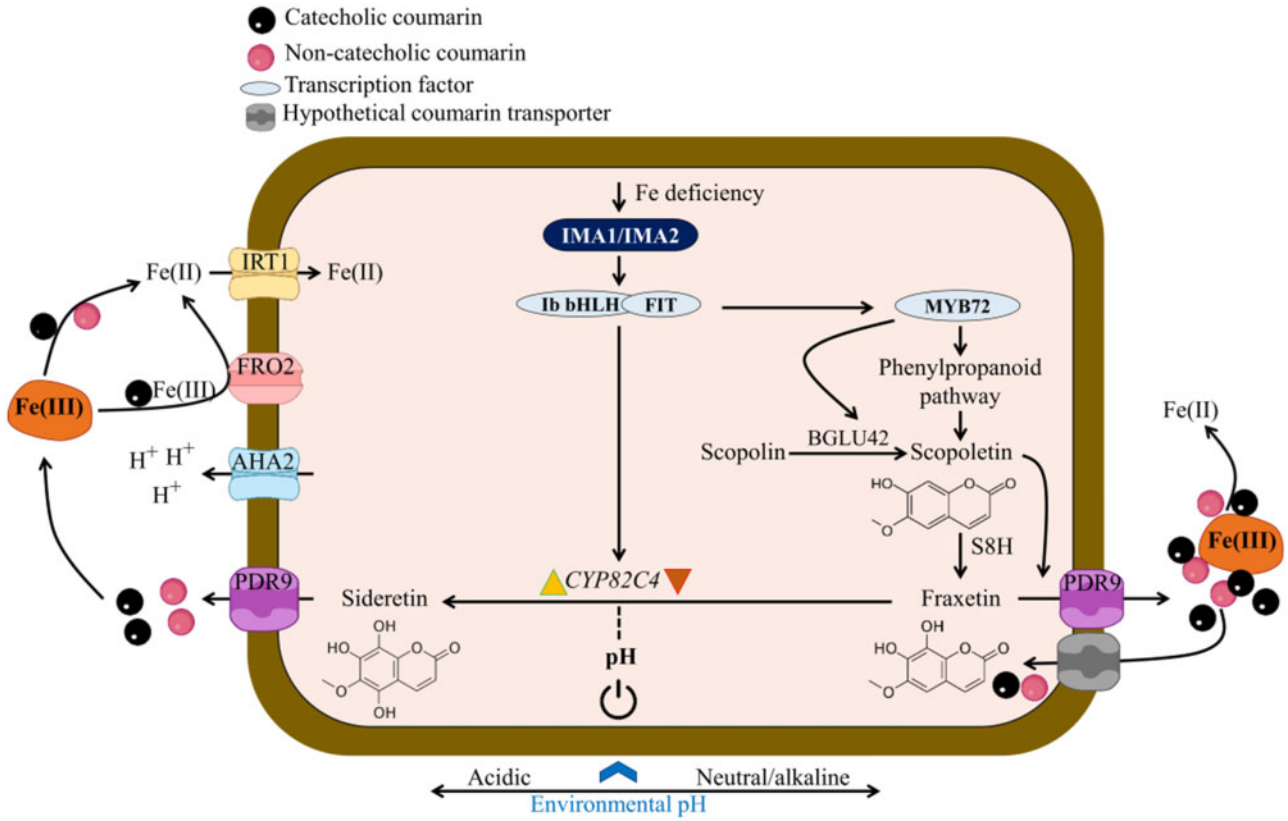

Figure 7 Model for the pH-dependent induction of the calcifuge (left) and calcicole (right) branches of the Fe-deficiency response. The expression of *IMA* genes is induced by a low Fe status of the plant, triggering the induction of two distinct suites of responses in correspondence with pH_e. Environmental pH dictates the biosynthesis of either sideretin or fraxetin by supporting the expression of *CYP82C4* at low pH_e and repressing *CYP82C4* transcription at elevated pH_e (indicated by yellow and brown arrowheads). At acidic pH, IMAs support the acquisition of Fe from Fe hydroxides by inducing proton extrusion, sideretin secretion, FCR, and uptake of Fe^{2+} via IRT1. The calcicole branch is positively regulated by MYB72. At neutral or alkaline pH ranges, IMAs induce the biosynthesis and secretion of fraxetin via PDR9, and Fe is mobilized via reduction and chelation. The β-glucosidase BGLU42 is prioritized over other BGLUs and required to facilitate the secretion of scopoletin, and presumably other coumarins, by catalyzing their deglycosylation. Re-uptake of coumarins into the roots as such or as a coumarin–Fe complex is mediated by an as yet unidentified transporter (Robe et al., 2020a). The two branches are not mutually exclusive, but prioritized by the prevailing pH_e. The blue arrow indicates a putative pH signal, tipping the balance (denoted by black circle) of induction (yellow arrowhead) and repression (brown arrowhead) of *CYP82C4*.

5 mM KNO_3, 2 mM $MgSO_4$, 2 mM $Ca(NO_3)_2$, 2.5 mM KH_2PO_4, 70 μM H_3BO_3, 14 μM $MnCl_2$, 1 μM $ZnSO_4$, 0.5 μM $CuSO_4$, 0.01 μM $CoCl_2$, 0.2 μM Na_2MoO_4, 1% (w/v) MES, and 1.5% (w/v) sucrose, solidified with 0.4% Gelrite pure (Kelco). Unless stated otherwise, media were supplemented with 50 μM Fe-EDTA or 400 μM Fe-EDTA (Fe excess; Fe^{2+}). The pH was adjusted to 5.5. Media with different Fe sources were prepared by replacing Fe-EDTA with 40 μM of either Fe-EDDHA, $FeCl_3$, or $Fe(OH)_3$. For Fe-deficient media, 120 μM ferrozine was added to the media. For preparing navFe media, 10 μM $FeCl_3$ was added as an Fe source and the pH was adjusted to 7.0 with KOH. For all media adjusted to pH 7.0, MOPS (1 g/L) was used as buffering agent instead of MES. Seeds were surface-sterilized with 30% (v/v) commercial bleach containing 6% NaClO and 70% (v/v) ethanol for 5 min, followed by five rinses with sterile MQ water, and stratified for 2 d in the dark at 4°C before transferring to a growth chamber. Plants were grown at 21°C under continuous illumination (50 μmol m^2s^{-1}). Soil of variable alkalinity was prepared by mixing 0.5% or 1% CaO (w/w) with peat-based soil.

RT-qPCR

Unless stated otherwise, 9-d-old plants were transferred from ES media to either fresh ES or navFe media for 3 d. At the end of the experimental period, samples were immediately frozen in liquid nitrogen and stored at −80°C. Total RNA was extracted using the RNeasy Mini Kit (Qiagen, Hilden, Germany) and treated with DNase using TURBO DNA-free kit (Ambion, Austin, TX, USA). cDNA was synthesized using DNA-free RNA with oligo-dT (20) primers and SuperScript III First-Strand Synthesis System for RT-qPCR (Invitrogen, Waltham, MA, USA). After incubation at 50°C for 1 h and 70°C for 15 min, 1 μL of RNase H was added and samples were incubated for 20 min at 37°C. The first-strand cDNA was used as a PCR template in a 10 μL reaction system using the SYBR Green PCR Master Mix (Applied Biosystems, Waltham, MA, USA) with programs

recommended by the manufacturer in an AB QuantStudio Real-Time PCR System (Applied Biosystems). Three independent replicates were performed for each sample. The ΔC_T method was used to determine the relative amount of gene expression, with the expression of elongation factor 1 alpha (EF1α; At5g60390) as an internal control. Primers used for RT-qPCR are listed in Supplemental Table 1.

Biomass and chlorophyll concentration

For biomass determination, whole shoots of 12- or 14-d-old seedlings grown on ES or navFe media were harvested and chlorophyll was extracted with 80% acetone. Total chlorophyll was calculated from absorbance measured at 645 and 663 nm using a protocol from Wellburn (1994).

Fe concentration

Total Fe concentration in shoots and roots was determined using a protocol described by Pan et al. (2015). Shoot and root samples (20–30 seedlings per sample) were oven-dried at 55°C for 2 d and digested with 65% (v/v) HNO_3 at 100°C for 6 h, followed by 30% (v/v) H_2O_2 at 56°C for 2 h. Digested samples were mixed in assay solution containing 1 mM bathophenanthroline disulfonate (BPDS), 0.6 M sodium acetate, and 0.48 M hydroxylamine hydrochloride. The concentration of the resulting Fe^{2+}–$BPDS_3$ complex was measured at A535 using a PowerWave XS2 microplate spectrophotometer (BioTek, Winooski, VT, USA). The Fe concentration in different samples was calculated by plotting OD values against a standard curve made with $FeCl_3$.

Perls staining for Fe(III)

Two-week-old Arabidopsis seedlings were vacuum infiltrated with Perls solution (2% HCl and 2% $K_4Fe(CN)_6$) for 30 min as described by Roschzttardtz et al. (2009). Samples were then rinsed 3 times with distilled water. Following staining, chlorophyll was removed from leaf samples with 80% acetone. Samples were rinsed thrice with distilled water and micrographs were taken with a Zeiss Lumar V12 Stereo microscope.

Rhizosphere acidification

For visualizing rhizosphere acidification, seedlings were germinated vertically on ES media with 0.5 g/L MES (instead of 1.0 g/L used in ES media) for 7 d and then carefully transferred to 1% BACTO™ agar media containing 0.006% Bromocresol Purple and 0.2 mM $CaSO_4$ for 24 h. The pH was adjusted to 6.1 with NaOH. Pictures were taken under white light at the end of the experimental period.

Ferric chelate reduction activity

In vivo root FCR activity was measured on 12-d-old seedlings after 3 d of growth on either Fe-replete or Fe-deplete media as described previously (Grillet et al., 2014). FCR activity was determined individually on roots of 5–10 intact seedlings. Plants were incubated in the dark for 30 min with mild shaking in a 2 mL assay solution consisting of 100 μM Fe-EDTA and 300 μM BPDS in 10 mM MES at pH 5.5. Spectrophotometric absorbance at 535 nm was recorded with a PowerWave XS2 plate reader (BioTek Instruments) to determine Fe^{2+}–$BPDS_3$ concentrations using a standard curve. Experiments were conducted at least 3 times independently.

Protein extraction and western blot analysis

Total protein from liquid-nitrogen-ground root tissues was extracted as described previously (Tsai et al., 2018). Equal amounts of total protein were loaded and separated on NuPAGE 4%–12% Bis–Tris gels (Invitrogen). Proteins were immune-detected using anti-IRT1 (Agrisera, Vännäs, Sweden; AS11 1780) or anti-S8H (Tsai et al., 2018) as primary antibodies followed by detection with secondary antibodies (Agrisera; AS09 602 and GE Healthcare, Chicago, IL, USA; A934-100UL, respectively). The chemiluminescence signal detection was performed using Pierce ECL Western Blotting Substrate (Thermo Fisher Scientific, Waltham, MA, USA) on X-ray film. Monoclonal anti-actin (plant) antibody detected by the secondary antibody (GE Healthcare; NA931-1ML) was used as a loading control (Sigma-Aldrich, St Louis, MO, USA; A0480).

Detection of fluorescent compounds in roots and media

The accumulation of fluorescent compounds in the roots and secreted into the media was visualized with a Bio Spectrum 600 imaging system (UVP) at 365 nm excitation wavelength, SYBR Gold 485 to 655 nm as emission filter, and exposure time set to 9 s as described previously (Tsai et al., 2018). The fluorescent intensity was quantified using the ImageJ tool. To record the UV–Vis spectra, a Varian Carry 5000 spectrophotometer equipped with a 1-cm quartz cuvette was used.

Coumarin extraction from roots and media

Coumarins were extracted following a protocol adapted from Tsai et al. (2018). For each sample, 18–20 roots frozen in liquid nitrogen were finely ground using glass beads in a Tissue Lyzer II (Qiagen). Subsequently, extraction was performed by adding 500 μL of 80% (v/v) methanol containing 0.5 ppm 4-methylumbelliferone as an internal standard into the finely ground samples. Samples were vigorously vortexed for 15 min. Following centrifugation at 13,200 rpm for 5 min, supernatants were collected in light-protected Eppendorf tubes. The pellets were subjected to re-extraction to obtain a final pooled volume of 1 mL. For coumarin extraction from growth media, roots were removed from the plates and the media were oven-dried at 50°C for 2 d, and subsequently incubated in 10 mL of 80% (v/v) methanol containing 0.1 ppm 4-methylumbelliferone for 30 min on a shaker. The extract was collected without disturbing the media debris. The extraction process was repeated twice. The samples were centrifuged at 13,200 rpm for 10 min and supernatants were used for targeted UPLC analysis.

Targeted coumarin analysis

Targeted coumarin profiling and data analysis was done as previously described (Tsai et al., 2018). UPLC–QTOF–MS analysis was performed on an Acquity UPLC system (Waters, Milford, MA, USA) and a SYNAPT G2 high-definition mass spectrometry system (Waters) with an electrospray ionization interface, ion mobility, and time-of-flight system. Spectra were collected in the positive ionization (ES+) mode. To obtain the relative coumarin levels, the metabolite peak area was normalized to the internal standard peak area and the number of roots.

Statistical analyses

All statistical analyses were conducted in R version 4.0.3 (R Core Team, 2020; https://www.eea.europa.eu/data-and-maps/indicators/oxygen-consuming-substances-in-rivers/r-development-core-team-2006). Data transformation and one/two-way analysis of variance were carried out with the reshape2 version 1.4.4 (Wickham, 2007), stats (R Core Team, 2020), and multcomp version 1.4-16 (Hothorn et al., 2008) packages, respectively. Post-hoc analysis was performed with function *TukeyHSD*; compact letter display of all pair-wise comparisons was obtained with *glht* function. Plots were generated with GraphPad Prism version 9.

Accession numbers

Arabidopsis genome initiative locus identifiers for the genes mentioned in this article are as follows: IMA1, At1g47400; IMA2, At1g47395; IMA3, At2g30766; IMA4, AT1G07367; IRP3, At2g14247; IRP4, At1g13609; IRP5, At3g56360; IRP6, At5g05250; AHA2, At4g30190; S8H, At3g12900; F6′H1, At3g13610; FIT, At2g28160; FRO2, At1g01580; IRT1, At4g19690; MYB72, At1g56160; CYP82C4, At4g31940; bHLH38, At3g56970, bHLH39, At3g56980; bHLH100, At2g41240; bHLH101, At5g04150; EF1α, At5g60390; BGLU42, At5g36890; PDR9, At3g53480; COSY, At1g28680; NAS4, At1g56430; bHLH18, At2g22750; bHLH19, At2g22760; bHLH20, At2g22770; bHLH25, At4g37850; URI, At3g19860; ILR3, At5g54680, BTSL1, At1g74770; and BTSL2, At1g18910, BGLU21, At1g66270; BGLU22, At1g66280; BGLU23, At3g09260.

Supplemental data

The following supplemental materials are available in the online version of this article.

Supplemental Table S1. Primers used in this study.

Supplemental Figure S1. Expression patterns of *IMA1* and *IMA2*.

Supplemental Figure S2. Perls staining of Col-0, *f6′h1-1*, *IMA1ox*, and *IMA2ox* seedlings.

Supplemental Figure S3. Phenotypes and Fe concentrations of Col-0, *f6′h1-1*, *IMA1ox*, and *IMA2ox* seedlings.

Supplemental Figure S4. Full scans of western blots.

Supplemental Figure S5. Autofluorescence of seedlings and media.

Supplemental Figure S6. pH dependence of scopoletin fluorescence.

Supplemental Figure S7. Phenotype and Fe concentration of wild-type seedlings grown on media supplemented with different Fe sources at pH 5.5 and pH 7.0.

Supplemental Figure S8. RT-qPCR analysis of key genes involved in Fe homeostasis.

Acknowledgments

The authors would like to thank Tushar S. Jadhav (Institute of Chemistry, Academia Sinica, Taipei) for insightful discussion on UV–Vis spectra analysis and Dr Louis Grillet (Department of Agricultural Chemistry, National Taiwan University, Taipei) for generating the *IMA2* overexpression lines without tag constructs. We thank the Plant Tech Core Facility at ABRC for protoplast isolation and transformation, the Small Molecule Metabolomics core facility, sponsored by the Institute of Plant and Microbial Biology, and the Scientific Instrument Center, Academia Sinica, for providing technical assistance, useful discussion, and support with data acquisition and analysis of Synapt HDMS experiments. We also acknowledge the use of the QuantStudio 12K Flex Real-Time PCR System at the Genomic Technology Core Facility at IPMB. The authors are most grateful for the continued support provided by Dr Wendar Lin from the Bioinformatics Core Facility at IPMB, Academia Sinica.

Funding

This work was supported by a grant from the Ministry of Science and Technology to W.S. (grant No.: 108-2311-B-001 -033 -MY3).

Conflict of interest statement. None declared.

References

Ahn YO, Shimizu BI, Sakata K, Gantulga D, Zhou Z, Bevan DR, Esen A (2010) Scopolin-hydrolyzing-glucosidases in roots of Arabidopsis. Plant Cell Physiol **51**: 132–143

Boxma, R (1981) Effect of pH on the behaviour of various iron chelates in sphagnum (moss) peat. Commun Soil Sci Plant Anal **12**: 755–763

Chen YT, Wang Y, Yeh KC (2017) Role of root exudates in metal acquisition and tolerance. Curr Opin Plant Biol **39**: 66–72

Clough SJ, Bent AF (1998) Floral dip: a simplified method for *Agrobacterium*-mediated transformation of *Arabidopsis thaliana*. Plant J **16**: 735–743

Colangelo EP, Guerinot ML (2004) The essential basic helix-loop-helix protein FIT1 is required for the iron deficiency response. Plant Cell **16**: 3400–3412

Cui Y, Chen CL, Cui M, Zhou WJ, Wu HL, Ling HQ (2018) Four IVa bHLH transcription factors are novel interactors of FIT and mediate JA inhibition of iron uptake in Arabidopsis. Mol Plant **11**: 1166–1183

Döll S, Kuhlmann M, Rutten T, Mette MF, Scharfenberg S, Petridis A, Berreth DC, Mock HP (2018) Accumulation of the coumarin scopolin under abiotic stress conditions is mediated by the Arabidopsis thaliana THO/TREX complex. Plant J **93**: 431–444

Eide D, Broderius M, Fettt J, Guerinott ML (1996) A novel iron-regulated metal transporter from plants identified by functional expression in yeast. Proc Natl Acad Sci USA **93**: 5624–5628

Estelle MA, Somerville C (1987) Auxin-resistant mutants of *Arabidopsis thaliana* with an altered morphology. MGG Mol Gen Genet **206**: 200–206

Fourcroy P, Sisó-Terraza P, Sudre D, Savirón M, Reyt G, Gaymard F, Abadía A, Abadia J, Álvarez-Fernández A, Briat JF (2014) Involvement of the ABCG37 transporter in secretion of scopoletin and derivatives by Arabidopsis roots in response to iron deficiency. New Phytol **201**: 155–167

Gao F, Robe K, Bettembourg M, Navarro N, Rofidal V, Santoni V, Gaymard F, Vignols F, Roschzttardtz H, Izquierdo E, et al. (2020) The transcription factor bHLH121 interacts with bHLH105 (ILR3) and its closest homologs to regulate iron homeostasis in Arabidopsis. Plant Cell **32**: 508–524

Grillet L, Lan P, Li W, Mokkapati G, Schmidt W (2018) IRON MAN is a ubiquitous family of peptides that control iron transport in plants. Nat Plants **4**: 953–963

Grillet L, Ouerdane L, Flis P, Hoang MTT, Isaure MP, Lobinski R, Curie C, Mari S (2014) Ascorbate efflux as a new strategy for iron reduction and transport in plants. J Biol Chem **289**: 2515–2525

Grime JP, Hodgson JG (1969) An investigation of the ecological significance of lime-chlorosis by means of large-scale comparative experiments. In IH Rorison, ed, Ecological Aspects of the Mineral Nutrition of Plants, Blackwell, Oxford, pp 67–99

Grusak MA, Welch RM, Kochian LV (1990) Does iron deficiency in *Pisum sativum* enhance the activity of the root plasmalemma iron transport protein? Plant Physiol **94**: 1353–1357

Harbort CJ, Hashimoto M, Inoue H, Niu Y, Guan R, Rombolà AD, Kopriva S, Voges MJEEE, Sattely ES, Garrido-Oter R et al. (2020) Root-secreted coumarins and the microbiota interact to improve iron nutrition in Arabidopsis. Cell Host Microbe **28**: 825–837.e6

Hirayama T, Lei GJ, Yamaji N, Nakagawa N, Ma JF (2018) The putative peptide gene FEP1 regulates iron deficiency response in Arabidopsis. Plant Cell Physiol **59**: 1739–1752

Hothorn T, Bretz F, Westfall P (2008) Simultaneous inference in general parametric models. Biometrical J **50**: 346–363

Jahn TP, Schulz A, Taipalensuu J, Palmgren MG (2002) Post-translational modification of plant plasma membrane H^+-ATPase as a requirement for functional complementation of a yeast transport mutant. J Biol Chem. **277**: 6353–6358

Kim SA, LaCroix IS, Gerber SA, Guerinot ML (2019) The iron deficiency response in *Arabidopsis thaliana* requires the phosphorylated transcription factor URI. Proc Natl Acad Sci USA **116**: 24933–24942

Kobayashi T, Nagano AJ, Nishizawa NK (2020) Iron deficiency-inducible peptide-coding genes OsIMA1 and OsIMA2 positively regulate a major pathway of iron uptake and translocation in rice. J Exp Bot **72**: 2196–2211

Lager I, Andréasson O, Dunbar TL, Andreasson E, Escobar MA, Rasmusson AG (2010) Changes in external pH rapidly alter plant gene expression and modulate auxin and elicitor responses. Plant Cell Environ **33**: 1513–1528

Lan P, Li W, Wen TN, Shiau JY, Wu YC, Lin W, Schmidt W (2011) ITRAQ protein profile analysis of Arabidopsis roots reveals new aspects critical for iron homeostasis. Plant Physiol **155**: 821–834

Lee JA (1998) The Calcicole-calcifuge problem revisited. Adv Bot Res **29**: 1–30

Lei R, Li Y, Cai Y, Li C, Pu M, Lu C, Yang Y, Liang G (2020) bHLH121 functions as a direct link that facilitates the activation of FIT by bHLH IVc transcription factors for maintaining Fe homeostasis in Arabidopsis. Mol Plant **13**: 634–649

Lin WD, Liao YY, Yang TJW, Pan CY, Buckhout TJ, Schmidt W (2011) Coexpression-based clustering of Arabidopsis root genes predicts functional modules in early phosphate deficiency signaling. Plant Physiol **155**: 1383–1402

Lucena C, Romera FJ, Rojas CL, García MJ, Alcántara E, Pérez-Vicente R (2007) Bicarbonate blocks the expression of several genes involved in the physiological responses to Fe deficiency of Strategy I plants. Funct Plant Biol **34**: 1002

Lucena JJ, Chaney RL (2006) Synthetic iron chelates as substrates of root ferric chelate reductase in green stressed cucumber plants. J Plant Nutr **29**: 423–439

Martín-Barranco A, Spielmann J, Dubeaux G, Vert G, Zelazny E (2020) Dynamic control of the high-affinity iron uptake complex in root epidermal cells. Plant Physiol **184**: 1236–1250

Meiser J, Lingam S, Bauer P (2011) Posttranslational regulation of the iron deficiency basic helix-loop-helix transcription factor FIT is affected by iron and nitric oxide. Plant Physiol **157**: 2154–2166

Nair RM, HanumanthaRao B, Vemula A, Rathore A, Brumbarova T, Ivanov R (2020) Availability of soil iron determines the distribution strategy and seed iron content in mungbean (*Vigna radiata*) plants. Plant Soil **446**: 413–423

Norvell WA (1991) Reactions of metal chelates in soils and nutrient solutions. *In* JJ Mortvedt, ed, Micronutrients in Agriculture, Soil Science Society of America, Madison, WI, pp 187–227

Obara K, Kihara A (2014) Signaling events of the Rim101 pathway occur at the plasma membrane in a ubiquitination-dependent manner. Mol Cell Biol **34**: 3525–3534

Palmer CM, Hindt MN, Schmidt H, Clemens S, Guerinot ML (2013) MYB10 and MYB72 are required for growth under iron-limiting conditions. PLoS Genet **9**: e1003953

Pan IC, Tsai HH, Cheng YT, Wen TN, Buckhout TJ, Schmidt W (2015) Post-transcriptional coordination of the *Arabidopsis* iron deficiency response is partially dependent on the E3 ligases RING DOMAIN LIGASE1 (RGLG1) and RING DOMAIN LIGASE2 (RGLG2). Mol Cell Proteomics **14**: 2733–2752

Peñalva MA, Lucena-Agell D, Arst HN (2014) Liaison alcaline: pals entice non-endosomal ESCRTs to the plasma membrane for pH signaling. Curr Opin Microbiol **22**: 49–59

Rajniak J, Giehl RFH, Chang E, Murgia I, Von Wirén N, Sattely ES (2018) Biosynthesis of redox-active metabolites in response to iron deficiency in plants. Nat Chem Biol **14**: 442–450

Raven JA (1990) Sensing pH? Plant, Cell Environ **13**: 721–729

Robe K, Conejero G, Gao F, Lefebvre-Legendre L, Sylvestre-Gonon E, Rofidal V, Hem S, Rouhier N, Barberon M, Hecker A et al. (2020a) Coumarin accumulation and trafficking in *Arabidopsis thaliana*: a complex and dynamic process. New Phytol **229**: 2062–2079

Robe K, Izquierdo E, Vignols F, Rouached H, Dubos C (2020b) The coumarins: secondary metabolites playing a primary role in plant nutrition and health. Trends Plant Sci **26**: 248–259

Robinson NJ, Procter CM, Connolly EL, Guerinot ML (1999) A ferric-chelate reductase for iron uptake from soils. Nature **397**: 694–697

Rodríguez-Celma J, Chun Pan I, Li W, Lan P, Buckhout TJ, Schmidt W (2013a) The transcriptional response of *Arabidopsis* leaves to Fe deficiency. Front Plant Sci **4**: 1–10

Rodríguez-Celma J, Connorton JM, Kruse I, Green RT, Franceschetti M, Chen YT, Cui Y, Ling HQ, Yeh KC, Balk J (2019) Arabidopsis BRUTUS-LIKE E3 ligases negatively regulate iron uptake by targeting transcription factor FIT for recycling. Proc Natl Acad Sci USA **116**: 17584–17591

Rodríguez-Celma J, Lin WD, Fu GM, Abadía J, López-Millán AF, Schmidt W (2013b) Mutually exclusive alterations in secondary metabolism are critical for the uptake of insoluble iron compounds by Arabidopsis and *Medicago truncatula*. Plant Physiol **162**: 1473–1485

Römheld V, Marschner H (1986) Evidence for a specific uptake system for iron phytosiderophores in roots of grasses. Plant Physiol **80**: 175–180

Roschzttardtz H, Conéjéro G, Curie C, Mari S (2009) Identification of the endodermal vacuole as the iron storage compartment in the Arabidopsis embryo. Plant Physiol **151**: 1329–1338

Santi S, Schmidt W (2009) Dissecting iron deficiency-induced proton extrusion in Arabidopsis roots. New Phytol **183**: 1072–1084

Schmid NB, Giehl RFH, Döll S, Mock HP, Strehmel N, Scheel D, Kong X, Hider RC, von Wirén N (2014) Feruloyl-CoA

6′-Hydroxylase1-dependent coumarins mediate iron acquisition from alkaline substrates in Arabidopsis. Plant Physiol **164**: 160–172

Schmidt W, Fühner C (1998) Sensitivity to and requirement for iron in *Plantago* species. New Phytol **138**: 639–651

Schwab AP, Lindsay WL (1983) Effect of redox on the solubility and availability of iron. Soil Sci Soc Am J **47**: 201–205

Shi WM, Chino M, Youssef RA, Mori S, Takagi S (1988) The occurrence of mugineic acid in the rhizosphere soil of barley plant. Soil Sci Plant Nutr **34**: 585–592

Sisó-Terraza P, Luis-Villarroya A, Fourcroy P, Briat JF, Abadía A, Gaymard F, Abadía J, Álvarez-Fernández A (2016) Accumulation and secretion of coumarinolignans and other coumarins in *Arabidopsis thaliana* roots in response to iron deficiency at high pH. Front Plant Sci **7**: 1711

Sivitz AB, Hermand V, Curie C, Vert G (2012) Arabidopsis bHLH100 and bHLH101 Control iron homeostasis via a FIT-independent pathway. PLoS One **7**: e44843

Siwinska J, Siatkowska K, Olry A, Grosjean J, Hehn A, Bourgaud F, Meharg AA, Carey M, Lojkowska E, Ihnatowicz A (2018) Scopoletin 8-hydroxylase: a novel enzyme involved in coumarin biosynthesis and iron-deficiency responses in Arabidopsis. J Exp Bot **69**: 1735–1748

Stringlis IA, De Jonge R, Pieterse CMJ (2019) The age of coumarins in plant-microbe interactions. Plant Cell Physiol **60**: 1405–1419

Stringlis IA, Yu K, Feussner K, De Jonge R, Van Bentum S, Van Verk MC, Berendsen RL, Bakker PAHM, Feussner I, Pieterse CMJ (2018) MYB72-dependent coumarin exudation shapes root microbiome assembly to promote plant health. Proc Natl Acad Sci USA **115**: E5213–E5222

Susín S, Abadía A, González-Reyes JA, Lucena JJ, Abadía J (1996) The pH requirement for *in vivo* activity of the iron-deficiency-induced "turbo" ferric chelate reductase: a comparison of the iron-deficiency-induced iron reductase activities of intact plants and isolated plasma membrane fractions in sugar beet. Plant Physiol **110**: 111–123

Terés J, Busoms S, Perez Martín L, Luís-Villarroya A, Flis P, Álvarez-Fernández A, Tolrà R, Salt DE, Poschenrieder C (2019) Soil carbonate drives local adaptation in *Arabidopsis thaliana*. Plant Cell Environ **42**: 2384–2398

Tsai HH, Schmidt W (2017) One way. Or another? Iron uptake in plants. New Phytol **214**: 500–505

Tsai HH, Schmidt W (2021) The enigma of environmental pH sensing in plants. Nat Plants **7**: 106–115

Tsai HH, Rodríguez-Celma J, Lan P, Wu YC, Vélez-Bermúdez IC, Schmidt W (2018) Scopoletin 8-hydroxylase-mediated fraxetin production is crucial for iron mobilization. Plant Physiol **177**: 194–207

Tsai HH, Schmidt W (2020) pH-dependent transcriptional profile changes in iron-deficient *Arabidopsis* roots. BMC Genomics **21**: 694

Tyler G (1996) Soil chemical limitations to growth and development of *Veronica officinalis* L. and *Carex pilulifera* L. Plant Soil **184**: 281–289

Vanholme R, Sundin L, Seetso KC, Kim H, Liu X, Li J, De Meester B, Hoengenaert L, Goeminne G, Morreel K, et al. (2019) COSY catalyses trans–cis isomerization and lactonization in the biosynthesis of coumarins. Nat Plants **5**: 1066–1075

Vert G, Grotz N, Dédaldéchamp F, Gaymard F, Guerinot M, Lou Briat JF, Curie C (2002) IRT1, an Arabidopsis transporter essential for iron uptake from the soil and for plant growth. Plant Cell **14**: 1223–1233

Voges MJEEE, Bai Y, Schulze-Lefert P, Sattely ES (2019) Plant-derived coumarins shape the composition of an *Arabidopsis* synthetic root microbiome. Proc Natl Acad Sci USA **116**: 12558–12565

Wang N, Cui Y, Liu Y, Fan H, Du J, Huang Z, Yuan Y, Wu H, Ling HQ (2013) Requirement and functional redundancy of Ib subgroup bHLH proteins for iron deficiency responses and uptake in *Arabidopsis thaliana*. Mol Plant **6**: 503–513

Waters BM, Amundsen K, Graef G (2018) Gene expression profiling of iron deficiency chlorosis sensitive and tolerant soybean indicates key roles for phenylpropanoids under alkalinity stress. Front Plant Sci **9**: 10

Wellburn AR (1994) The spectral determination of chlorophylls a and b, as well as total carotenoids, using various solvents with spectrophotometers of different resolution. J Plant Physiol **144**: 307–313

Wickham H (2007) Reshaping data with the reshape package. J Stat Softw **21**: 1–20 [Database]

Yuan Y, Wu H, Wang N, Li J, Zhao W, Du J, Wang D, Ling HQ (2008) FIT interacts with AtbHLH38 and AtbHLH39 in regulating iron uptake gene expression for iron homeostasis in Arabidopsis. Cell Res **18**: 385–397

Zamioudis C, Hanson J, Pieterse CMJ (2014) β-Glucosidase BGLU42 is a MYB72-dependent key regulator of rhizobacteria-induced systemic resistance and modulates iron deficiency responses in Arabidopsis roots. New Phytol **204**: 368–379

Ziegler J, Schmidt S, Strehmel N, Scheel D, Abel S (2017) Arabidopsis transporter ABCG37/PDR9 contributes primarily highly oxygenated coumarins to root exudation. Sci Rep **7**: 1–11

Zohlen A, Tyler G (2004) Soluble inorganic tissue phosphorus and calcicole-calcifuge behaviour of plants. Ann Bot **94**: 427–432